Chemical abundances of three new Ba stars from the Keck/HIRES spectra

Shuai Liu (刘帅)[1,2], Liang Wang (王靓)[3,4], Jian-Rong Shi (施建荣)[1,2], Zhen-Yu Wu (武振宇)[1,2],
Hong-Liang Yan (闫宏亮)[1,2], Qi Gao (高琦)[1,2] and Chun-Qian Li (李春乾)[1,2]

[1] CAS Key Laboratory of Optical Astronomy, National Astronomical Observatories, Chinese Academy of Sciences, Beijing 100101, China; *sjr@nao.cas.cn*

[2] School of Astronomy and Space Science, University of Chinese Academy of Sciences, Beijing 100049, China

[3] National Astronomical Observatories/Nanjing Institute of Astronomical Optics & Technology, Chinese Academy of Sciences, Nanjing 210042, China

[4] CAS Key Laboratory of Astronomical Optics & Technology, Nanjing Institute of Astronomical Optics & Technology, Chinese Academy of Sciences, Nanjing 210042, China

Abstract Based on high resolution, high signal-to-noise (S/N) ratio spectra from Keck/HIRES, we have determined abundances of 20 elements for 18 Ba candidates. The parameter space of these stars is in the range of $4880 \leq T_{\mathrm{eff}} \leq 6050$ K, $2.56 \leq \log g \leq 4.53$ dex and $-0.27 \leq$ [Fe/H] ≤ 0.09 dex. It is found that four of them can be identified as Ba stars with [s/Fe] > 0.25 dex (s: Sr, Y, Zr, Ba, La, Ce and Nd), and three of them are newly discovered, which include two Ba giants (HD 16178 and HD 22233) and one Ba subgiant (HD 2946). Our results show that the abundances of α, odd and iron-peak elements (O, Na, Mg, Al, Si, Ca, Sc, Ti, Mn, Ni and Cu) for our program stars are similar to those of the thin disk, while the distribution of [hs/ls] (hs: Ba, La, Ce and Nd, ls: Sr, Y and Zr) ratios of our Ba stars is similar to those of the known Ba objects. None of the four Ba stars show clear enhancement in carbon including the known CH subgiant HD 4395. It is found that three of the Ba stars present clear evidence of hosting stellar or sub-stellar companions from the radial velocity data.

Key words: Galaxy — Ba stars — Chemical abundances — Binary

1 INTRODUCTION

Barium stars are a type of particular objects, which were first discovered by Bidelman & Keenan (1951), and exhibit strong spectral lines from slow neutron capture process (s-process) elements (such as Sr, Y, Zr, La, Ce, Pr, Nd or Sm) and CH, CN and C_2 molecules. Early on, it was noted that Ba stars are G/K-type giants. Later, similar spectral features have been found in some CH subgiant (Bond 1974) and dwarf stars (North et al. 1994), these objects are called Ba dwarfs. It is well known that the s-process nucleosynthesis happens in the thermal pulse Asymptotic Giant Branch (TP-AGB) (e.g., Busso et al. 1999; Herwig 2005; Käppeler et al. 2011; Karakas & Lattanzio 2014) stage, in which the inner materials are carried to the surface by the Third Dredge-Up (TDU) mechanism. However, the observed luminosities of Ba stars failed to attain the threshold to trigger this stage (Escorza et al. 2017; Bergeat & Knapik 1997). Thus, this type stars have enhanced their heavy elements by the mechanism of self-enrichment.

McClure et al. (1980) discovered that the radial velocities of their nine of 11 strong Ba stars present periodic variations, and suggested that those objects may have a companion. Subsequently, observations on the variances of radial velocities (e.g., McClure 1983; McClure & Woodsworth 1990; Jorissen et al. 1998) and UV excess (e.g., Bohm-Vitense et al. 1984; Böhm-Vitense et al. 2000; Gray et al. 2011) for some Ba stars confirmed this suggestion, and indicated that the companion star is quite possible a white dwarf. Therefore, a deduction could be drawn that Ba stars formed by the accretion of heavy elements from a companion, which have already undergone the TP-AGB stage (e.g., McClure et al. 1980; Han et al. 1995).

Recently, some works have noted that the degrees of Ba enrichment may be influenced by the distance between the two stars (Han et al. 1995; Antipova et al. 2004; Yang et al. 2016), or the metallicities (Jorissen et al. 1998), the latter plays a critical role on the s-process nucleosynthesis of second-to-first peak elements in AGB stars (Gallino et al. 1998; Goriely & Mowlavi 2000). According to the

evolutionary timescales and the orbital characteristics of Ba stars (North et al. 2000) and the cooling times of white dwarfs (Böhm-Vitense et al. 2000), it can be inferred that most Ba stars are contaminated while in the main sequence, which means that the progenitor star of a Ba giant might be a Ba dwarf. However, the mass distribution of the observed Ba dwarfs ($M < 2M_{\odot}$) peaks at much lower mass compared to those of Ba giants ($M > 2M_{\odot}$), and Ba dwarfs have a distribution tending to more metal-poor than that of Ba giants ($-0.1 <$ [Fe/H] < 0.1), which means that the Ba dwarfs we have observed do not represent the progenitor of the Ba giants (Escorza et al. 2019; Jorissen et al. 2019). Some researches have found that Ba stars can also exist in triple systems, such as HD 48565 and HD 114520 (North et al. 2000; Escorza et al. 2019).

Heavy elements beyond Fe group can also be produced by fast neutron capture process (r-process), however, the stellar site of main r-process is still in debate. The candidate sites include the neutrino-driven wind of core collapse supernovae (CCSNe, Wanajo 2013), the magneto-hydrodynamically driven jet from rapidly rotating, strongly magnetized CCSNe (Winteler et al. 2012), and neutron star mergers (e.g. Argast et al. 2004). In some metal-poor stars, the abundance pattern shows an obvious enrichment of heavy elements between the s- and r-processes (Barbuy et al. 1997; Jonsell et al. 2006), which is called i-process (Cowan & Rose 1977). Therefore, Ba stars perhaps have more complicated mechanism of enrichment.

Chemical abundance is an invaluable tool to probe the nucleosynthetic process, and the [hs/ls] ratio has been widely used to investigate the efficiency of the s-process (Luck & Bond 1991; Smiljanic et al. 2007). Here 'hs' represents the mean value of the heavy s-process element abundances (Ba, La, Ce and Nd), while 'ls' is for light elements (Sr, Y, Zr). The theoretical models arrived at, after AGB stage, the ratios of ls, hs and [hs/ls] decrease with increasing metallicity during $-1.5 <$ [Fe/H] < 0 dex for stars with mass between 1.5 $M_{\odot}$ and 3 $M_{\odot}$ (Busso et al. 2021). Smiljanic et al. (2007) found that the strong Ba stars have higher [hs/ls] than those of the mild Ba stars, and de Castro et al. (2016) showed that the [s/Fe] and [hs/ls] ratios are strongly anticorrelated with the metallicity (also see Kong et al. 2018). It is suggested by Shejeelammal & Goswami (2020) that the ratio of [Rb/Zr] is an important diagnostic index for understanding the average neutron density in the s-process site and the mass of the AGB stars, the [Rb/Zr] ratio is negative for low-mass AGB stars, while it is positive for intermediate-mass AGB stars (e.g. van Raai et al. 2012).

Based on the strength of the Ba II resonance line at 4554 Å, Warner (1965) classified the Ba stars from the scale 0 (weakest) to 5 (strongest), and Lu (1991) noted that the strong Ba stars of scale $= 2-5$ belong to the old disk with a large dispersion in space velocities, while the weak ones of scale < 2 are generally young disk objects with a small scatter in space velocities. Although, de Castro et al. (2016) noted that the Ba stars could not be sorted through the [s/Fe] ratios clearly, he suggested that a value of [s/Fe] =li 0.25 dex is the minimal ratio for an object identified as a Ba star. Compared to the mild Ba stars, strong ones generally have lower metallicities (Kovacs 1985), and tend to have shorter periods (Jorissen et al. 2019).

Up to now, only a small number of Ba stars have been certified especially for Ba dwarfs. The catalog of 389 Ba giants listed by Lu (1991) including certain and candidate samples, and some of them have no heavy-element overabundances (Jorissen et al. 1996). de Castro et al. (2016) gathered 182 Ba giant candidates, and confirmed 169 of them with s-process elements enhanced. Kong et al. (2018) have collected 58 Ba CH subgiant and dwarf stars with abundance information including their three new Ba dwarfs, however, the number is still smaller compared to the Ba giants. Therefore, it is important to enlarge the sample for understanding the formation and evolution of Ba dwarfs.

In previous work, we have found 18 Ba candidate stars based on analyzing the high resolution, high signal-to-noise-ratio spectra from Keck/HIRES (Liu et al. 2020). In this paper, we have derived the detailed elemental abundances and radial velocities for the 18 Ba candidates by analyzing the HIRES high-resolution spectra. The outline of this paper is as follows. In Section 2, we will briefly introduce the key information about the spectra and our program stars. The stellar atmospheric parameters of our program stars are presented in Section 3. In Section 4 we show the detailed elemental abundances, and the results of the elemental abundances and radial velocities are discussed in Section 5. The conclusions are drawn in Section 6.

2 THE SPECTRA AND SAMPLE STARS

The High Resolution Echelle Spectrometer (HIRES) is a high resolution visible light slit spectrograph installed at the 10 m Keck telescope in 1996 (Vogt et al. 1994), and it was used by the California Planet Search program team to obtain high resolution spectrum with an average resolution of R $\approx$ 60 000 and high precision radial velocities of ~1-3 m s^{-1} (CPS; Howard et al. 2010). The precise radial velocities are obtained by installing an iodine molecule (I$_2$) vapor cell with constant temperature ($50.0 \pm 0.1°$C) in front of the slit. The I$_2$ imprints a series of weak absorption lines over the stellar spectrum, which can be used to precisely calibrate the wavelength (Valenti et al. 1995; Butler et al. 1996). The wavelength coverages of the spectra are divided into three sections of 3640 to 4790 Å, 4970 to 6420 Å and 6540 to 7980 Å. All of the spectra
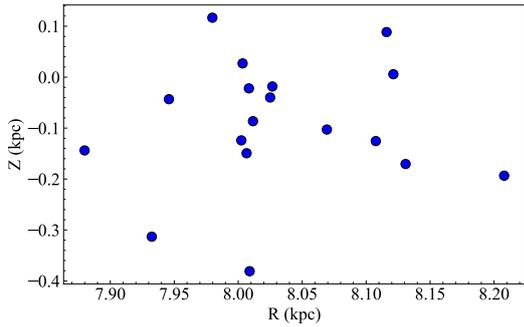
Fig. 1 The distribution of our sample stars in the R−Z plane.

Table 1 The Stellar Parameters of Our Sample Stars

Star Name	T_{eff}	$\log g$	[Fe/H]	$\xi_t(\mathrm{km\,s^{-1}})$	S/N
HD 2946	5570	3.70	−0.27	1.11	80
HD 3458	5018	2.71	−0.06	1.10	86
HD 4395	5494	3.61	−0.15	0.85	84
HD 11131	5845	4.53	0.00	0.70	130
HD 12484	5835	4.50	0.09	1.08	140
HD 16178	4900	2.72	−0.09	1.15	99
HD 18015	5603	3.64	−0.11	1.05	90
HD 18645	5458	3.36	0.08	1.20	92
HD 22233	5172	3.11	−0.03	0.90	95
HD 38949	6050	4.50	−0.04	1.00	93
HD 45210	5717	3.54	−0.07	1.10	89
HD 72440	5600	3.60	−0.08	1.00	86
HD 103847	5209	4.52	0.03	0.80	152
HD 108189	5273	3.20	−0.09	0.95	93
HD 200491	5083	2.90	0.03	1.05	68
HD 205163	4989	3.00	0.09	1.13	85
HD 220122	4880	2.56	−0.18	1.08	93
HD 224679	5677	3.55	0.08	1.05	86

in this study were taken from the HIRES archive, and the signal-to-noise (S/N) ratios for the spectra are listed in the last column of Table 1.

The 18 Ba candidates have been selected from our previous work (Liu et al. 2020), which presented the Ba abundance of 602 objects derived from the spectra collected from CPS. Our sample includes the star HD 4395, which was identified as a CH subgiant in previous studies (e.g. Busso et al. 1999; de Castro et al. 2016). Figure 1 gives the spatial distribution in R − Z plane for the program stars. Here, we use the 1/parallax as the distance of a star, and the parallax comes from the Gaia EDR3 catalog (Gaia Collaboration et al. 2021). As shown in Figure 1, these stars lie in the solar vicinity, and most likely belong to the thin disk.

3 THE STELLAR ATMOSPHERE PARAMETERS

In this paper, the stellar parameters of all 18 stars have been revised via the spectroscopic approach, e.g. the effective temperature is determined by fulfilling the excitation equilibrium of Fe I, the surface gravity is obtained by the ionization equilibrium of Fe I and Fe II, and the microturbulence velocity is derived by forcing [Fe/H] from different Fe I lines to be independent of their equivalent widths. This process of deriving stellar parameters is an iterative procedure, and the initial data from Brewer et al. (2016) is applied. In our analysis, 33 Fe I and 12 Fe II unblended optical lines selected from Yan et al. (2018) have been adopted, and the information of these lines is shown in Table A.1. It is noted that the departures from local thermal equilibrium (LTE) of Fe I lines are small, lower than 0.05 dex for our sample stars (Lind et al. 2012; Sitnova et al. 2015), therefore, the non-local thermal equilibrium (NLTE) effects have not been considered when determining the iron abundance.

Figure 2 shows the derived abundances from individual Fe I and Fe II lines as functions of their equivalent widths (left panel) and excitation potentials (right panel) for a typical star of HD 45210. The final stellar parameters of our 18 samples are presented in Table 1. Based on

multiple iterative processes, we estimate that the typical uncertainties of T_{eff}, $\log g$, [Fe/H], and ξ_t are $\pm 80\,\mathrm{K}$, $\pm 0.1\,\mathrm{dex}$, $\pm 0.1\,\mathrm{dex}$, and $0.2\,\mathrm{km\,s^{-1}}$, respectively.

We also determine the surface gravities ($\log g$) adopted the parallax from the Gaia EDR3 (Gaia Collaboration et al. 2021) using Girardi's online code PARAM 1.3[1] (da Silva et al. 2006). As shown in Figure 3, there is a good agreement between these two values, and the mean scatter is about 0.07.

4 ANALYSIS OF ELEMENT ABUNDANCES

4.1 Atomic Data

In our work, the line list along with the atomic data of C I, Na I, Mg I, Al I, Si I, Ca I, Sc II, Ti II, Cu I, Zr II, Sr II and Ba II is taken from Zhao et al. (2016), and we adopted the solar abundances recommended by Asplund et al. (2009). The oxygen abundance is derived by fitting the forbidden [O I] line at 6300 Å, which blended with a Ni I line, and the $\log gf$ values of the forbidden [O I] line and Ni I line at 6300 Å are adopted from Centeno & Socas-Navarro (2008). Meanwhile, the line list of Mn I, Ni I, Sr I, Y II, La II, Ce II, Nd II and Eu II is selected from Roederer et al. (2018), and we revise the ($\log gf$) values by fitting the solar spectrum with LTE assumption. The detailed information is listed in Table A.1. In addition, the hyperfine structure (HFS) plays an important role for strong absorption lines, and HFS of Sc (Lawler et al. 2019), Cu (Shi et al. 2014), Mn (Den Hartog et al. 2011), La (Ivans et al. 2006) and Eu (Lawler et al. 2001) has been taken into account.

4.2 Elemental Abundances and Their Uncertainties

For all elements, the abundances of our program stars were determined using the spectral synthesis method, and the

---

[1] *http://stev.oapd.inaf.it/cgi-bin/param_1.3*
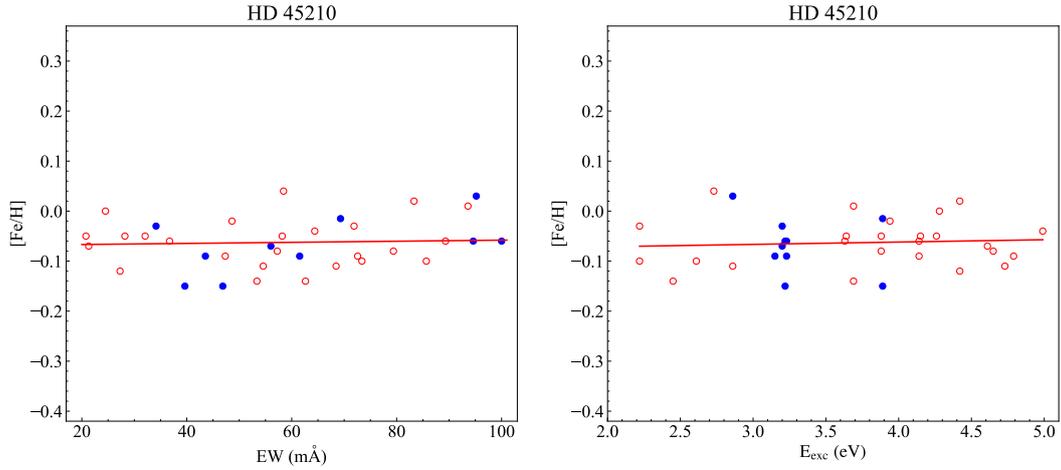
Fig. 2 The determination of stellar parameters of a typical star, HD 45210, based on the ionization and excitation equilibrium of Fe I and Fe II lines. *Open red circles* refer to Fe I lines and *filled (blue) circles* to Fe II lines. The *red straight lines* are the fitting results with a least square method.
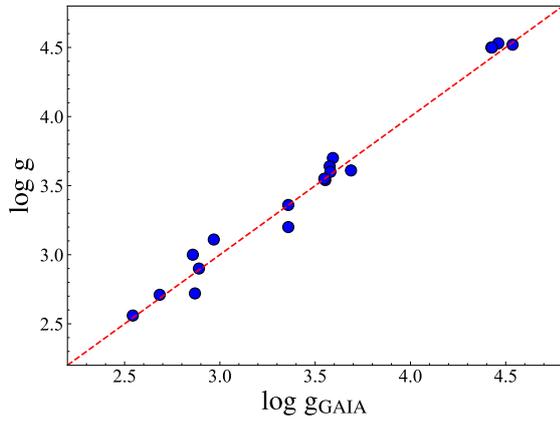
Fig. 3 The difference of the $\log g$ determined with our method and those calculated by PARAM.

one dimensional LTE MAFAGS opacity sampling (OS) models in plane-parallel atmospheres (Grupp 2004; Grupp et al. 2009) have been adopted. It is noted by Reddy & Lambert (2017) that the barium abundances are over-estimated by the standard LTE methods, our previous work (Liu et al. 2020) has also presented that the non-local thermodynamic equilibrium (NLTE) effects cannot be neglected, and the barium abundances can be over-estimated by up to 0.2 dex compared to the NLTE analysis. Thus, the NLTE effects have been considered in this work when deriving barium abundances.

An interactive IDL code Spectrum Investigation Utility (SIU, Reetz 1991) is used to perform the line formation. In order to fit the observed spectral lines, we handled the broadenings due to the rotation, macro-turbulence and instrument as one single Gauss profile to be convolved with the synthetic spectra. It needs to be pointed out that our sample stars are not fast rotators.

The final abundances of 20 elements (C, O, Na, Mg, Al, Si, Ca, Sc, Ti, Mn, Ni, Cu, Sr, Y, Zr, Ba, La, Ce, Nd and Eu) are given in Table B.1 ([Sr I/Fe] ratio represents the mean value of [Sr I/Fe] and [Sr II/Fe] ratios), and the uncertainties presented are the statistical standard deviation of different spectral lines for each element. In Figure 4 we have plotted [X/Fe] v.s. the atomic number Z for the 18 stars in our sample.

It needs to be pointed out that only one line in our spectrum range is suitable to derive chemical abundance for each of the following six elements, e.g., C, Sr, Zr, La, Nd and Eu. Due to the poor quality of the Sr II lines at 4077 Å and 4215 Å, we used the Sr I and Sr II lines at 4607 and 4161 Å, respectively, to derive the abundance of this element.

The uncertainties in the stellar parameters (T_{eff}, $\log g$, [Fe/H] and ξ_t) will lead to the errors of elemental abundances, and we select one typical star of HD 16178 to investigate this impact. The errors in elemental abundances due to the uncertainties of 100 K in T_{eff}, 0.2 dex in $\log g$, 0.1 dex in [Fe/H] and 0.2 km s^{-1} in ξ_t are presented in Table 2. The last column lists the square roots of the quadratic sum of the errors associated with all the four factors. As shown in the Table, the uncertainties due to one of the stellar parameters are less than 0.10 dex for most of the elements. The abundances of O and Sr are sensitive to temperature, while the strong lines of Ti, Ni, Sr and Ba are sensitive to micro-turbulence.

4.3 Comparing to Previous Works

In order to validate our results on the element abundances, we compared them with those from previous works. Brewer et al. (2016) gave the abundances of 15 elements, which have 13 common elements with our study. To
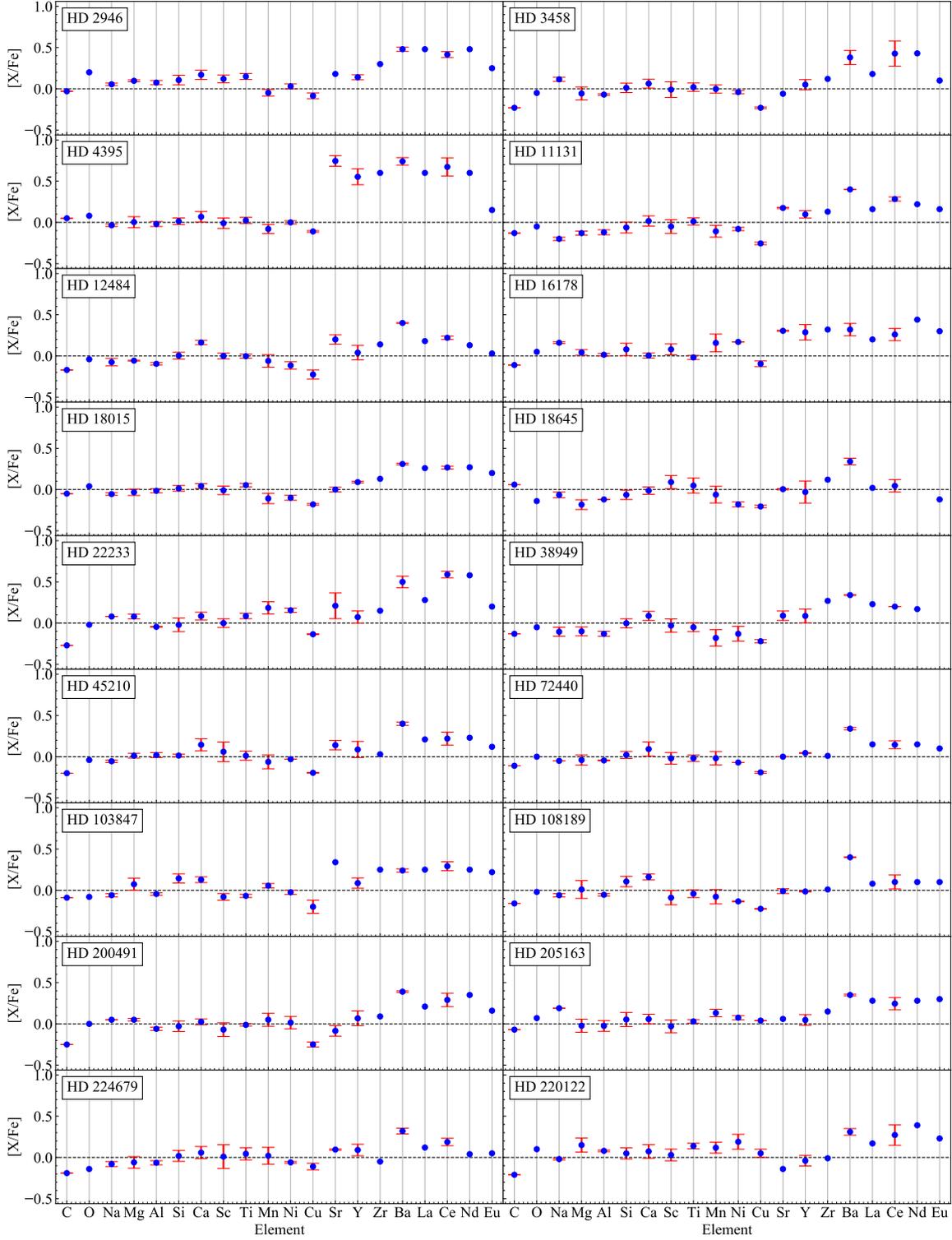
Fig. 4 The elemental abundances of our 18 sample stars.

avoid the uncertainties due to different atmospheric stellar parameters adopted, we compared the abundance results only for the ten objects with $\Delta T_{\mathrm{eff}} < 100\,\mathrm{K}$, $\Delta \log g < 0.1\,\mathrm{dex}$ and $\Delta[\mathrm{Fe/H}] < 0.1\,\mathrm{dex}$. The comparison results are presented in Figure 5, and it shows that the mean deviation is lower than 0.1 dex for all elements.

We notice that the abundances of s-process elements for two stars, HD 103847 and HD 4395, have been determined by Tabernero et al. (2012) and Karinkuzhi &

Table 2 Estimated Uncertainties in Abundance Analysis for One Example Star of HD 16178

Δ [X/Fe]	ΔT_{eff} +100 K	$\Delta \log g$ +0.2 dex	Δ [Fe/H] +0.1 dex	$\Delta \xi_t$ +0.2 km s^{-1}	$\Delta Total$
C I	-0.07	$+0.07$	-0.10	$+0.02$	$+0.14$
O I	-0.15	$+0.09$	-0.09	-0.02	$+0.20$
Na I	$+0.07$	-0.02	-0.10	-0.04	$+0.13$
Mg I	$+0.06$	-0.01	-0.08	-0.08	$+0.13$
Al I	$+0.08$	$+0.02$	-0.07	$+0.01$	$+0.10$
Si I	-0.01	$+0.04$	-0.07	-0.03	$+0.09$
Ca I	$+0.05$	-0.04	-0.06	-0.10	$+0.13$
Sc II	$+0.01$	$+0.10$	-0.06	-0.07	$+0.14$
Ti II	$+0.00$	$+0.07$	-0.07	-0.11	$+0.15$
Mn I	$+0.10$	$+0.01$	-0.03	-0.08	$+0.13$
Ni I	$+0.09$	$+0.03$	-0.05	-0.14	$+0.17$
Cu I	$+0.05$	$+0.01$	-0.07	-0.08	$+0.11$
Sr I	$+0.18$	$+0.00$	-0.08	-0.12	$+0.23$
Sr II	$+0.06$	$+0.10$	-0.04	-0.07	$+0.14$
Zr II	-0.04	$+0.09$	-0.07	-0.06	$+0.13$
Ba II	$+0.03$	-0.13	-0.05	-0.12	$+0.18$
Eu II	-0.02	$+0.08$	-0.05	-0.03	$+0.10$
Y II	$+0.00$	$+0.08$	-0.04	-0.07	$+0.11$
La II	$+0.04$	$+0.09$	-0.04	$+0.01$	$+0.11$
Ce II	$+0.03$	$+0.08$	-0.03	-0.08	$+0.12$
Nd II	$+0.05$	$+0.07$	-0.04	-0.06	$+0.11$

Table 3 The Comparison of the Abundances of s-process Elements for HD 103847 and HD 4395

Star Name	[Sr I/Fe]	[Y II/Fe]	[Zr II/Fe]	[Ba II/Fe]	[La II/Fe]	[Ce II/Fe]	[Nd II/Fe]	Remarks
HD 103847	0.34	0.09	0.25	0.24	0.25	0.29	0.25	Our work
	—	0.16	0.10	0.19	—	0.27	0.25	T12
HD 4395	0.79	0.55	0.60	0.86	0.60	0.67	0.60	Our work
	1.08	0.65	0.58	0.79	1.03	0.42	0.80	K14

Notes: T12: Tabernero et al. (2012); K14: Karinkuzhi & Goswami (2014).
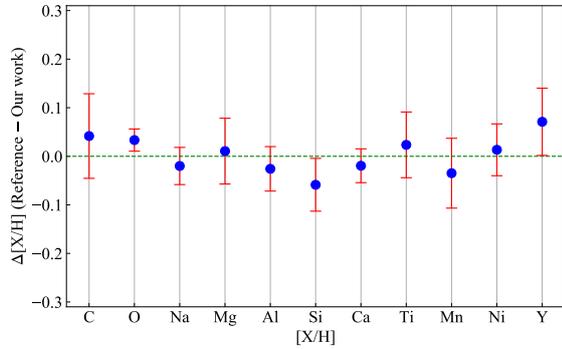
Fig. 5 The differences of elemental abundances between ours and Brewer et al. (2016). Only the objects with ΔT_{eff} < 100 K, $\Delta \log g$ < 0.1 dex and Δ[Fe/H]) < 0.1 dex have been selected, which contains 10 common stars.

Goswami (2014), respectively. The differences between our values and those of the references are presented in Figure 6 (also see Table 3). As shown in the figure, our values have a good agreement with those of Tabernero et al. (2012) for HD 103847, while they are large discrepancy of Sr, La, Sr and Nd for HD 4395 (Karinkuzhi & Goswami 2014). We find that the stellar atmosphere parameters adopted for HD 4395 are very similar for ours and those from Karinkuzhi & Goswami (2014). It is noted that the Sr abundances are derived from the only Sr I line at 4607.33 Å for both works,
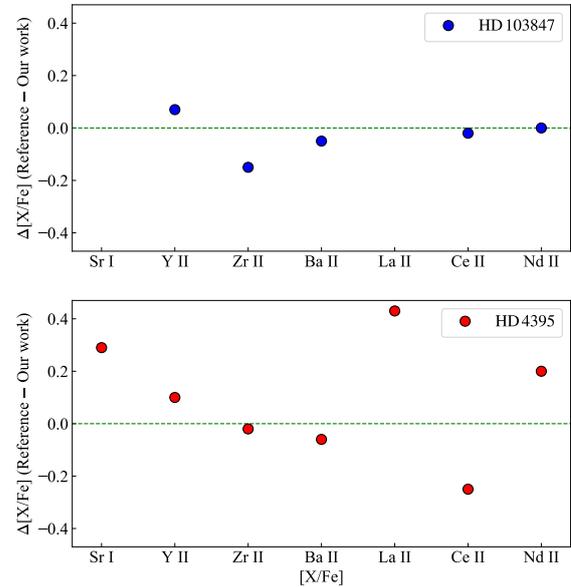
Fig. 6 The comparison of the difference in the s-process elemental abundances for two common stars of HD 103847 and HD 4395 studied by Tabernero et al. (2012) and Karinkuzhi & Goswami (2014), respectively.

and the corresponding difference in $\log gf$ values is -0.62 ($\log gf_{\mathrm{Ref.}} = -0.57$, $\log gf_{\mathrm{our}} = 0.28$). Thus, the deviation can partially be explained by the different $\log gf$ values adopted. Moreover, the Sr abundances of 13 sample
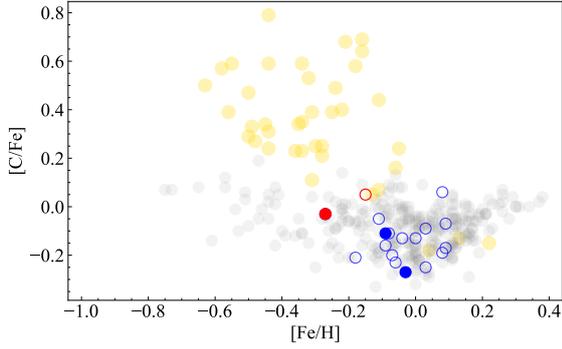
Fig. 7 The [C/Fe] ratio plotted against metallicity. The *filled blue* and *red circles* are our newly discovered Ba giants and subgiant, respectively. The *open blue* and *red circles* are the known CH subgiant HD 4395 and 14 comparison stars, respectively. The *grey dots* are the field FGK dwarfs from da Silva et al. (2015), and the *yellow dots* are for the known Ba dwarfs and CH subgiants from Kong et al. (2018).

Fig. 9 The [Eu/Fe] ratio against metallicity. The *blue* and *red circles* are the same as Fig. 7, while the *yellow* and *cyan dots* are the thin- and thick-disk stars from Bensby et al. (2005).

5 DISCUSSION

5.1 Identification of Ba Stars

As previously mentioned, de Castro et al. (2016) suggested a minimal value of [s/Fe] = 0.25 as a criterion to identify Ba stars. According to this rule, four objects in our sample can be classified as Ba stars including one known CH subgiant of HD 4395 ([s/Fe] = 0.65), and three are newly discovered e.g. HD 2946 ([s/Fe] = 0.35), HD 16178 ([s/Fe] = 0.31) and HD 22233 ([s/Fe] = 0.36). Among these three new Ba stars, HD 16178 and HD 22233 are Ba giants with $\log g = 3.11$ and 2.72, respectively, while HD 2946 is a Ba subgiant with $\log g = 3.70$. For the rest of 14 stars, they all show Ba enhancement of [Ba/Fe] > 0.3 except for HD 103847, the latter has a [s/Fe] value of 0.24 dex, which is close to the standard of Ba stars. Thus, these 14 stars, which contain six dwarfs and eight giants, are added as a reference in the following discussion.

5.2 Carbon Abundances

The first Ba stars identified by Bidelman & Keenan (1951) is enhancement of carbon, and according to the classical Ba star scenario, carbon can be produced in the form of ^{12}C by shell He burning in TP-AGB stage (Porto de Mello & da Silva 1997). Figure 7 shows the ratio of [C/Fe] vs. metallicity, and there is no significant enrichment of carbon found in our sample stars, including the known CH subgiant of HD 4395 ([C/Fe] = 0.05). The distribution of [C/Fe] of the program stars follows the galactic field dwarfs.

Fig. 8 The [hs/ls] ratios plotted against metallicity. The *blue* and *red circles* have the same meaning as Fig. 7. The *yellow dots* are the known Ba dwarfs and CH subgiants from Kong et al. (2018), and the *cyan dots* is the known Ba giants from de Castro et al. (2016).

5.3 The Abundances of α, Odd and Iron Group Elements

As shown in Figure 4, most sample stars have similar chemical abundances in Na, Al, Sc α- and iron-peak elements (Na, Mg, Al, Si, Ca, Sc, Ti, Mn and Ni). We

stars are also derived with the Sr II line at 4161 Å, and the mean deviation from the [Sr I/Fe] and [Sr II/Fe] is 0.06 dex. For the abundance of Ce, we have one common Ce II line at 5330.56 Å, and the difference in $\log gf$ value is −0.46 ($\log gf_{\mathrm{Ref.}} = -0.76$, $\log gf_{\mathrm{our}} = -0.30$). We also check the equivalent widths of this line, and the values are 12.7 mÅ (Ref.) and 15.6 mÅ (this work), respectively. Our Ce abundance is obtained from four Ce II lines, and they give consistent abundance results, while theirs are based on only two lines. The abundance differences in La and Nd are hard to discuss, as there are no common lines for these two works.

Fig. 10 The radial velocities of our four Ba stars.

notice that the abundances of copper are slightly lower, which may be explained by the NLTE effect. According to former research (Shi et al. 2014; Xu et al. 2019), the NLTE effect for copper is about +0.05 dex.

5.4 The Abundances of s-process Elements

The [hs/ls] ratio is a powerful tool to diagnose the efficiency of s-process (Luck & Bond 1991), here, [hs] and [ls] are the mean abundances of the heavy (Ba, La, Ce and Nd) and light s-process elements (Sr, Y and Zr), respectively. Recently, Kong et al. (2018) have found that the [hs/ls] ratios show an anti-correlation with metallicity for CH subgiant and dwarf Ba stars. Figure 8 presents the ratios of [hs/ls] as a function of metallicity, and for comparison we also include the samples from de Castro et al. (2016) and Kong et al. (2018). As shown in the bottom panel of Figure 8, the [hs/ls] ratios of the three new Ba stars are consistent with those of the known Ba stars, and the subgiant Ba star of HD 2946 tends having higher [hs/ls] value than that of the most known Ba dwarfs at the same metallicity. As highlighted in Kong et al. (2018), an anti-correlation existed between [hs/ls] and metallicity

in the sample of Ba dwarfs and CH subgiants, while this relevance is not obvious for Ba giants.

In addition, with regard to the 14 Ba candidates, no matter giants or dwarfs, the distribution of [hs/ls] ratios is similar to the known Ba giants.

5.5 The Abundances of r-process Element Eu

It has been found that europium mainly comes from the r-process (e.g., Cescutti et al. 2006), and the [Eu/Fe] ratio is a diagnostic to determine whether the r-process dominated the nucleosynthesis at a given moment of the evolution of the Galaxy. At very low metallicities, the r-process is expected to be the dominate heavy element production, since the massive stars first explode in the form of nuclear collapse and enrich the interstellar medium (ISM) before the AGB stars participate in the main s-process. In this work, we also derived the Eu abundances, and the results are presented in Figure 9. We can see that the Eu abundances of our Ba stars are similar to those of the thick-disk stars.

5.6 Radial Velocities of the Four Ba Stars

In this work, we acquired the high precise radial velocities of our four Ba stars by using the public online code of HIRES Precision Radial Velocity Pipeline[2] (Marcy & Butler 1992; Butler et al. 1996; Howard et al. 2010). The typical uncertainty of radial velocities is around 1–3 m s^{-1}.

The variations of radial velocities for the four Ba stars are presented in Figure 10. It can be found that three stars (HD 4395, HD 16178 and HD 22233) have obvious secular linear trends on radial velocities, suggesting the existences of long-period companions around these stars. The acceleration ($|\dot{\gamma}|$) are between 20 to 70 m s^{-1} yr^{-1}. It is difficult to estimate the minimum mass of the companions with the existing radial velocity data. Their companions can be either planet, brown dwarf, or low-mass stars. Long-term monitoring are essential to uncover their properties. For HD 2946, no linear radial velocity trends are observed. We also calculate the Generalized Lomb-Scargle periodogram (Zechmeister & Kürster 2009) of the radial velocity data, and did not find any significant peak with False Alarm Probability (FAP) less than 10^{-3}, which means there is no clue of hosting stellar or substellar companions. However, binarity of Ba subgiant HD 2946 cannot be excluded. High spatial-resolution imaging will be helpful to reveal their possible companions.

6 CONCLUSIONS

In this work, based on the high resolution and high S/N spectra from Keck/HIRES, we have determined the abundances of 20 elements (C, O, Na, Mg, Al, Si, Ca, Sc, Ti, Mn, Ni, Cu, Sr, Y, Zr, Ba, La, Ce, Nd and Eu) for 18 Ba candidates. The parameter space for our sample stars are in the range of $4880 \leq T_{\mathrm{eff}} \leq 6050$ K, $2.56 \leq \log g \leq 4.53$ dex and $-0.27 \leq$ [Fe/H] ≤ 0.09 dex. The conclusions are as follows.

- We confirm that four of our 18 Ba candidates are Ba stars, and three of them are newly discovered including one Ba subgiant of HD 2946 and two Ba giants of HD 16178 and HD 22233.
- Three of our four Ba stars, HD 4395, HD 16178 and HD 22233, have clear evidence of hosting stellar or sub-stellar companions in long-term radial velocity data, and the binarity for the Ba subgiant HD 2946 cannot be excluded.
- The distribution of the [hs/ls] ratios for all of four Ba stars is similar to that of the known Ba objects, and our results support the suggestion that there is an anti-correlation between the [hs/ls] ratio and metallicity for CH subgiant and dwarf Ba stars.

- No significant enrichment of carbon is found for our Ba stars, including the known CH subgiant HD 4395.

Combining more observations on the radial velocities and photometric in longer time range, we could further solve the orbit parameters of the binaries. In addition, it is important to search for more metal-poor Ba stars ([Fe/H] < -0.6) and metal-rich Ba dwarfs ([Fe/H] > -0.1]) to investigate the relation between the [hs/ls] ratios and metallicities.

Appendix A: ABSORPTION LINES USED FOR ABUNDANCE DETERMINATION

Appendix B: THE ELEMENTAL ABUNDANCES OF OUR SAMPLE STARS

References

Antipova, L. I., Boyarchuk, A. A., Pakhomov, Y. V., & Panchuk, V. E. 2004, Astronomy Reports, 48, 597

Argast, D., Samland, M., Thielemann, F. K., & Qian, Y. Z. 2004, A&A, 416, 997

Table A.1 Absorption Lines Used for Abundance Determination

Ion	λ (Å)	χ (eV)	log *gf*
C I	5380.33	7.68	−1.62
O I	6300.30	0	−9.78
Na I	6154.23	2.10	−1.55
	6160.75	2.10	−1.25
Mg I	4571.09	0.00	−5.47
	4730.03	4.34	−2.20
	5711.07	4.34	−1.64
Al I	6696.03	3.14	−1.51
	6698.67	3.14	−1.87
Si I	5690.42	4.71	−1.74
	5701.10	4.71	−1.96
	5772.15	5.08	−1.62
	6142.48	5.62	−1.48
	6145.02	5.62	−1.39
	6155.13	5.62	−0.78
	6237.32	5.61	−1.08
	6243.81	5.62	−1.29
	6244.47	5.62	−1.29
Ca I	5512.98	2.93	−0.46
	5867.57	2.93	−1.57
	6161.29	2.51	−1.27
	6166.44	2.51	−1.14
	6169.06	2.51	−0.80
	6169.56	2.53	−0.48
Sc II	5031.02	1.35	−0.41
	5641.00	1.49	−0.99
	5657.90	1.50	−0.54
	5669.04	1.49	−1.10
	5684.19	1.50	−1.03
Ti II	4470.85	1.16	−2.02
	4583.41	1.16	−2.84
	4708.66	1.24	−2.35
	5336.79	1.58	−1.60
	5418.77	1.58	−2.13
Mn I	4761.51	2.95	−0.27
	4765.85	2.94	−0.09
	6013.51	3.07	−0.35
	6021.82	3.07	−0.05
Fe I	4574.22	2.28	−2.37
	5242.50	3.63	−0.83
	5295.32	4.42	−1.54
	5379.58	4.15	−1.35
	5576.10	3.43	−0.76
	5633.95	4.99	−0.19
	5638.27	4.22	−0.70
	5662.52	4.18	−0.45
	5679.02	4.65	−0.68
	5705.48	4.30	−1.44
	5814.81	4.28	−1.85
	5852.22	4.55	−1.20
	5855.08	4.61	−1.55
	5916.25	2.45	−2.87
	5930.18	4.65	−0.18
	6024.06	4.55	+0.08
	6056.01	4.73	−0.36
	6065.49	2.61	−1.41
	6079.01	4.65	−0.97
	6127.90	4.14	−1.36
	6151.62	2.18	−3.26
	6165.36	4.14	−1.44
	6173.34	2.22	−2.82
	6180.20	2.73	−2.66
	6200.32	2.61	−2.32

Table A.1 *Continued*

Ion	λ (Å)	χ (eV)	log *gf*
Fe I	6213.43	2.22	−2.45
	6232.64	3.65	−1.12
	6252.55	2.40	−1.58
	6393.61	2.43	−1.43
	6593.87	2.44	−2.28
	6609.11	3.56	−2.58
	6733.15	4.64	−1.44
	6750.15	2.42	−2.54
Fe II	4508.28	2.86	−2.37
	4520.22	2.81	−2.60
	5197.58	3.22	−2.54
	5234.63	3.22	−2.24
	5264.81	3.22	−3.06
	5414.07	3.22	−3.57
	5425.26	3.20	−3.28
	5991.38	3.15	−3.60
	6084.11	3.20	−3.83
	6149.25	3.89	−2.74
	6247.56	3.89	−2.56
	7711.73	3.90	−2.58
Ni I	6300.34	4.27	−2.11
	6643.63	1.68	−2.22
	6767.77	1.82	−2.14
Cu I	5105.54	1.39	−1.52
	5218.20	3.82	0.48
Sr I	4607.33	0.00	0.28
Sr II	4161.79	2.94	−0.50
Y II	5087.42	1.08	−0.16
	5402.77	1.84	−0.31
	5544.61	1.74	−0.83
Zr II	5112.27	1.66	−0.85
Ba II	5853.67	0.60	−1.00
	6141.71	0.70	−0.08
La II	6390.48	0.32	−1.41
Ce II	4562.36	0.48	0.21
	4572.28	0.68	0.22
	4628.16	0.52	0.14
	5330.56	0.87	−0.40
Nd II	5319.81	0.55	−0.14
Eu II	6645.06	1.38	0.12

Asplund, M., Grevesse, N., Sauval, A. J., & Scott, P. 2009, ARA&A, 47, 481

Barbuy, B., Cayrel, R., Spite, M., et al. 1997, A&A, 317, L63

Bensby, T., Feltzing, S., Lundström, I., & Ilyin, I. 2005, A&A, 433, 185

Bergeat, J., & Knapik, A. 1997, A&A, 321, L9

Bidelman, W. P., & Keenan, P. C. 1951, ApJ, 114, 473

Böhm-Vitense, E., Carpenter, K., Robinson, R., et al. 2000, ApJ, 533, 969

Bohm-Vitense, E., Nemec, J., & Proffitt, C. 1984, ApJ, 278, 726

Bond, H. E. 1974, ApJ, 194, 95

Brewer, J. M., Fischer, D. A., Valenti, J. A., & Piskunov, N. 2016, ApJS, 225, 32

Busso, M., Gallino, R., & Wasserburg, G. J. 1999, ARA&A, 37, 239

Busso, M., Vescovi, D., Palmerini, S., Cristallo, S., & Antonuccio-Delogu, V. 2021, ApJ, 908, 55

Butler, R. P., Marcy, G. W., Williams, E., et al. 1996, PASP, 108,

500

Centeno, R., & Socas-Navarro, H. 2008, ApJL, 682, L61

Cescutti, G., François, P., Matteucci, F., Cayrel, R., & Spite, M. 2006, A&A, 448, 557

Cowan, J. J., & Rose, W. K. 1977, ApJ, 212, 149

da Silva, L., Girardi, L., Pasquini, L., et al. 2006, A&A, 458, 609

da Silva, R., Milone, A. d. C., & Rocha-Pinto, H. J. 2015, A&A, 580, A24

de Castro, D. B., Pereira, C. B., Roig, F., et al. 2016, MNRAS, 459, 4299

Den Hartog, E. A., Lawler, J. E., Sobeck, J. S., Sneden, C., & Cowan, J. J. 2011, ApJS, 194, 35

Escorza, A., Boffin, H. M. J., Jorissen, A., et al. 2017, A&A, 608, A100

Escorza, A., Karinkuzhi, D., Jorissen, A., et al. 2019, A&A, 626, A128

Gaia Collaboration, Brown, A. G. A., Vallenari, A., et al. 2021, A&A, 649, A1

Gallino, R., Arlandini, C., Busso, M., et al. 1998, ApJ, 497, 388

Goriely, S., & Mowlavi, N. 2000, A&A, 362, 599

Gray, R. O., McGahee, C. E., Griffin, R. E. M., & Corbally, C. J. 2011, AJ, 141, 160

Grupp, F. 2004, A&A, 420, 289

Grupp, F., Kurucz, R. L., & Tan, K. 2009, A&A, 503, 177

Han, Z., Eggleton, P. P., Podsiadlowski, P., & Tout, C. A. 1995, MNRAS, 277, 1443

Herwig, F. 2005, ARA&A, 43, 435

Howard, A. W., Johnson, J. A., Marcy, G. W., et al. 2010, ApJ, 721, 1467

Ivans, I. I., Simmerer, J., Sneden, C., et al. 2006, ApJ, 645, 613

Jonsell, K., Barklem, P. S., Gustafsson, B., et al. 2006, A&A, 451, 651

Jorissen, A., Boffin, H. M. J., Karinkuzhi, D., et al. 2019, A&A, 626, A127

Jorissen, A., Schmitt, J. H. M. M., Carquillat, J. M., Ginestet, N., & Bickert, K. F. 1996, A&A, 306, 467

Jorissen, A., Van Eck, S., Mayor, M., & Udry, S. 1998, A&A, 332, 877

Käppeler, F., Gallino, R., Bisterzo, S., & Aoki, W. 2011, Reviews of Modern Physics, 83, 157

Karakas, A. I., & Lattanzio, J. C. 2014, PASA, 31, e030

Karinkuzhi, D., & Goswami, A. 2014, MNRAS, 440, 1095

Kong, X. M., Bharat Kumar, Y., Zhao, G., et al. 2018, MNRAS, 474, 2129

Kovacs, N. 1985, A&A, 150, 232

Lawler, J. E., Hala, Sneden, C., et al. 2019, ApJS, 241, 21

Lawler, J. E., Wickliffe, M. E., den Hartog, E. A., & Sneden, C. 2001, ApJ, 563, 1075

Lind, K., Bergemann, M., & Asplund, M. 2012, MNRAS, 427, 50

Liu, S., Shi, J., & Wu, Z. 2020, ApJ, 896, 64

Lu, P. K. 1991, AJ, 101, 2229

Luck, R. E., & Bond, H. E. 1991, ApJS, 77, 515

Marcy, G. W., & Butler, R. P. 1992, PASP, 104, 270

McClure, R. D. 1983, ApJ, 268, 264

McClure, R. D., Fletcher, J. M., & Nemec, J. M. 1980, ApJL, 238, L35

McClure, R. D., & Woodsworth, A. W. 1990, ApJ, 352, 709

North, P., Berthet, S., & Lanz, T. 1994, A&A, 281, 775

North, P., Jorissen, A., & Mayor, M. 2000, in The Carbon Star Phenomenon, ed. R. F. Wing, Vol. 177, 269

Porto de Mello, G. F., & da Silva, L. 1997, ApJL, 476, L89

Reddy, A. B. S., & Lambert, D. L. 2017, ApJ, 845, 151

Reetz, J. K. 1991, Diploma thesis, Universität München

Roederer, I. U., Sakari, C. M., Placco, V. M., et al. 2018, ApJ, 865, 129

Shejeelammal, J., & Goswami, A. 2020, Journal of Astrophysics and Astronomy, 41, 37

Shi, J. R., Gehren, T., Zeng, J. L., Mashonkina, L., & Zhao, G. 2014, ApJ, 782, 80

Sitnova, T., Zhao, G., Mashonkina, L., et al. 2015, ApJ, 808, 148

Smiljanic, R., Porto de Mello, G. F., & da Silva, L. 2007, A&A, 468, 679

Tabernero, H. M., Montes, D., & González Hernández, J. I. 2012, A&A, 547, A13

Valenti, J. A., Butler, R. P., & Marcy, G. W. 1995, PASP, 107, 966

van Raai, M. A., Lugaro, M., Karakas, A. I., et al. 2012, A&A, 540, A44

Vogt, S. S., Allen, S. L., Bigelow, B. C., et al. 1994, in Society of Photo-Optical Instrumentation Engineers (SPIE) Conference Series, 2198, Instrumentation in Astronomy VIII, eds. D. L. Crawford & E. R. Craine, 362

Wanajo, S. 2013, ApJL, 770, L22

Warner, B. 1965, MNRAS, 129, 263

Winteler, C., Käppeli, R., Perego, A., et al. 2012, ApJL, 750, L22

Xu, X. D., Shi, J. R., & Yan, H. L. 2019, ApJ, 875, 142

Yan, H.-L., Shi, J.-R., Zhou, Y.-T., et al. 2018, Nature Astronomy, 2, 790

Yang, G.-C., Liang, Y.-C., Spite, M., et al. 2016, RAA (Research in Astronomy and Astrophysics), 16, 19

Zechmeister, M., & Kürster, M. 2009, A&A, 496, 577

Zhao, G., Mashonkina, L., Yan, H. L., et al. 2016, ApJ, 833, 225

Table B.1 The Elemental Abundances of Our Sample Stars

Star Name	[C/Fe]	error	[O/Fe]	error	[Na/Fe]	error	[Mg/Fe]	error	[Al/Fe]	error	[Si/Fe]	error	[Ca/Fe]	error	[Sc/Fe]	error	[Ti/Fe]	error	[Mn/Fe]	error
HD 2946	−0.03	—	0.13	0.059	0.06	0.015	0.10	0.012	0.08	0.025	0.11	0.058	0.17	0.056	0.12	0.047	0.15	0.036	−0.05	0.040
HD 3458	−0.23	—	0.18	0.071	0.12	0.025	−0.06	0.079	−0.07	0.010	0.03	0.057	0.06	0.054	−0.01	0.094	0.02	0.051	0.00	0.050
HD 4395	0.05	—	0.10	0.043	−0.04	0.015	0.00	0.066	−0.02	0.030	0.01	0.040	0.07	0.063	−0.01	0.063	0.02	0.037	−0.08	0.055
HD 11131	−0.13	—	0.09	0.111	−0.20	0.020	−0.13	0.024	−0.12	0.030	−0.06	0.067	0.02	0.062	−0.05	0.083	0.01	0.044	−0.11	0.071
HD 12484	−0.17	—	0.04	0.090	−0.08	0.045	−0.06	0.005	−0.10	0.015	0.00	0.042	0.16	0.026	0.00	0.035	0.00	0.025	−0.06	0.076
HD 16178	−0.11	—	0.23	0.111	0.16	0.010	0.04	0.034	0.02	0.015	0.08	0.075	0.01	0.031	0.08	0.067	−0.02	0.025	0.16	0.108
HD 18015	−0.05	—	0.16	0.083	−0.06	0.015	−0.03	0.039	−0.02	0.025	0.01	0.035	0.04	0.029	−0.01	0.052	0.05	0.021	−0.11	0.063
HD 18645	0.06	—	0.13	0.102	−0.07	0.035	−0.18	0.059	−0.12	0.000	−0.06	0.057	−0.01	0.045	0.09	0.080	0.05	0.091	−0.06	0.101
HD 22233	−0.27	—	−0.04	0.076	0.08	0.000	0.08	0.028	−0.05	0.005	−0.02	0.082	0.09	0.048	0.00	0.053	0.09	0.032	0.19	0.074
HD 38949	−0.13	—	0.05	0.069	−0.11	0.055	−0.10	0.054	−0.13	0.030	0.00	0.055	0.09	0.055	−0.03	0.081	−0.05	0.053	−0.18	0.100
HD 45210	−0.20	—	0.01	0.024	−0.06	0.015	0.01	0.029	0.02	0.030	0.01	0.018	0.15	0.073	0.06	0.119	0.01	0.055	−0.06	0.084
HD 72440	−0.11	—	0.01	0.038	−0.05	0.000	−0.04	0.062	−0.05	0.005	0.02	0.042	0.10	0.087	−0.02	0.071	−0.02	0.039	−0.02	0.081
HD 103847	−0.09	—	0.05	0.029	−0.06	0.020	0.07	0.073	−0.05	0.015	0.14	0.056	0.13	0.035	−0.08	0.041	−0.07	0.019	0.06	0.027
HD 108189	−0.16	—	0.23	0.093	−0.06	0.020	0.01	0.018	−0.06	0.015	0.11	0.063	0.16	0.037	−0.09	0.086	−0.04	0.046	−0.08	0.087
HD 200491	−0.25	—	−0.01	0.071	0.05	0.000	0.05	0.016	−0.06	0.020	−0.03	0.063	0.03	0.035	−0.07	0.083	−0.01	0.015	0.05	0.079
HD 205163	−0.07	—	0.29	0.127	0.19	0.000	−0.02	0.079	−0.03	0.065	0.05	0.085	0.06	0.058	−0.03	0.078	0.03	0.021	0.13	0.045
HD 220122	−0.21	—	0.15	0.057	−0.02	0.010	0.15	0.086	0.08	0.010	0.05	0.068	0.07	0.083	0.03	0.071	0.14	0.034	0.12	0.066
HD 224679	−0.19	—	0.09	0.095	−0.08	0.030	−0.06	0.070	−0.07	0.025	0.02	0.066	0.06	0.074	0.01	0.145	0.04	0.074	0.02	0.102

Star Name	[Ni/Fe]	error	[Cu/Fe]	error	[Sr I/Fe]	error	[Sr II/Fe]	error	[Y/Fe]	error	[Zr/Fe]	error	[Ba/Fe]	error	[La/Fe]	error	[Ce/Fe]	error	[Nd/Fe]	error	[Eu/Fe]	error
HD 2946	0.03	0.030	−0.09	0.035	0.18	—	—	—	0.14	0.030	0.30	—	0.48	0.025	0.48	—	0.42	0.036	0.48	—	0.25	—
HD 3458	−0.04	0.020	−0.23	0.010	−0.06	—	—	—	0.05	0.062	0.12	—	0.38	0.085	0.18	—	0.43	0.152	0.43	—	0.10	—
HD 4395	0.00	0.020	−0.11	0.010	0.79	—	0.70	—	0.55	0.096	0.60	—	0.86	0.045	0.60	—	0.67	0.110	0.60	—	0.15	—
HD 11131	−0.08	0.020	−0.26	0.015	0.18	—	0.17	—	0.10	0.045	0.13	—	0.40	0.000	0.16	—	0.28	0.025	0.22	—	0.16	—
HD 12484	−0.12	0.045	−0.23	0.055	0.24	—	0.16	—	0.04	0.088	0.14	—	0.40	0.005	0.18	—	0.22	0.020	0.13	—	0.03	—
HD 16178	0.17	0.000	−0.10	0.035	0.31	—	0.30	—	0.29	0.094	0.32	—	0.32	0.075	0.20	—	0.26	0.074	0.44	—	—	—
HD 18015	−0.10	0.030	−0.18	0.010	0.02	—	−0.02	—	0.09	0.010	0.13	—	0.31	0.010	0.26	—	0.27	0.017	0.27	—	0.20	—
HD 18645	−0.18	0.030	−0.21	0.015	0.01	—	0.00	—	−0.03	0.134	0.12	—	0.34	0.040	0.02	—	0.05	0.075	—	—	−0.12	—
HD 22233	0.16	0.025	−0.14	0.005	0.32	—	0.1	—	0.07	0.074	0.15	—	0.50	0.070	0.28	—	0.50	0.167	0.58	—	0.20	—
HD 38949	−0.13	0.090	−0.22	0.020	0.13	—	0.05	—	0.09	0.084	0.27	—	0.34	0.005	0.23	—	0.20	0.000	0.17	—	—	—
HD 45210	−0.03	0.000	−0.20	0.005	0.18	—	0.1	—	0.09	0.098	0.03	—	0.40	0.020	0.21	—	0.22	0.079	0.23	—	0.12	—
HD 72440	−0.07	0.000	−0.19	0.010	0.00	—	0.00	—	0.05	0.005	0.01	—	0.34	0.015	0.15	—	0.15	0.048	0.15	—	0.10	—
HD 103847	−0.03	0.025	−0.20	0.080	0.34	—	—	—	0.09	0.063	0.25	—	0.24	0.020	0.25	—	0.29	0.054	0.25	—	0.22	—
HD 108189	−0.14	0.005	−0.23	0.005	0.01	—	−0.03	—	−0.02	0.005	0.01	—	0.40	0.005	0.08	—	0.10	0.085	0.10	—	0.10	—
HD 200491	0.02	0.075	−0.25	0.030	−0.04	—	−0.13	—	0.07	0.090	0.09	—	0.39	0.010	0.21	—	0.29	0.081	0.35	—	0.16	—
HD 205163	0.08	0.025	0.04	0.000	0.06	—	—	—	0.05	0.065	0.15	—	0.35	0.010	0.28	—	0.25	0.074	0.28	—	0.30	—
HD 220122	0.19	0.090	0.05	0.050	−0.14	—	—	—	−0.04	0.064	−0.01	—	0.31	0.040	0.18	—	0.27	0.124	0.39	—	0.23	—
HD 224679	−0.06	0.010	−0.11	0.040	0.10	—	0.09	—	0.09	0.070	−0.05	—	0.32	0.035	0.12	—	0.19	0.045	0.04	—	0.05	—